Long-range impact localization with a frequency domain triangulation technique: Application to a large aircraft composite panel

Dimitri Goutaudier, Didier Gendre, Veronique Kehr-Candille, Roger Ohayon

Long-range impact localization with a frequency domain triangulation technique: Application to a large aircraft composite panel

Dimitri Goutaudier[a,b,c,*], Didier Gendre[b], Véronique Kehr-Candille[a], Roger Ohayon[c]

[a] *Onera, Department of Materials and Structures, Châtillon, France*
[b] *Airbus, Airport Operations, Blagnac, France*
[c] *Cnam, Structural Mechanics and Coupled Systems Lab., Paris, France*

Abstract

Classical triangulation techniques determine the impact point by capturing the Time of Arrival (TOA) delays of some elastic waves at different sensor locations. This paper presents an impact localization technique that exploits the low frequency content of the global vibration response. A modal signature of the impact location is described instead of a time signature based on the TOAs. The proposed approach uses the simple idea that the vibration modes of a structure are not excited in the same proportions depending on impact location. The proposed method is applied to a large aircraft composite panel equipped with a sparse distribution of accelerometers. An experimental modal analysis was performed prior to the impact tests to identify the first low frequency vibration modes of the structure within 10-50Hz. The results of the study show that the technique succesfully localizes impacts applied at any location on the panel.

Keywords: Structural Health Monitoring, impact localization, vibration analysis, composite panel

1. Introduction

It is now well-known that impacts on composite panels may produce internal damages without obvious external evidence [1, 2, 3]. Since composites are widely used in aerospace structures, reporting impact events is an important task of Structural Health Monitoring. A potential enabler would be an impact monitoring system that could detect when and where an impact occurred. Hence it would be faster to check the structure's integrity with a non-destructive technique [4] as the impact location would be known prior to the inspection.

In the literature, various techniques have been developed to determine the impact location from measurements of sensors installed on the target structure. Since an impact generates elastic waves propagating in the structure [5], many wave-based localization techniques have been proposed. These techniques consist in detecting the Time Of Arrival (TOA) delays of specific elastic waves at the sensor locations to triangulate the impact point. Zhao et al. [6] used the antisymmetric Lamb wave mode A_0 [7] to triangulate an impact event on a Carbon Fiber Reinforced Polymer (CFRP) plate equipped with 4 strain gauges. First, they detected the TOAs of A_0 waves with a wavelet transform analysis of the measured signals. Then, they numerically solved a nonlinear set of equations to estimate the coordinates of the impact point. However the applicability of this method on complex structures is limited as the wave velocity model relies on the structural geometry and the properties of the propagation media. To overcome this difficulty, Frieden et al. [8] used a reference data set to infer the impact location on a CFRP plate equipped with 4 FBG sensors. First, the TOAs of A_0 Lamb waves were estimated with a threshold method. Then, each pair of TOA was converted into an iso-propagation line with an interpolation technique using the reference data set. The intersection of these lines finally gave an estimation of the impact location. Many methods based on Artificial Neural Networks (ANNs) have also been proposed to triangulate the impact location without any assumption on the propagation media. ANNs are mathematical models that can be trained with a reference data set to model a nonlinear relationship between inputs and outputs. Zhong et al. [9] used an ANN trained with 50 reference impact tests to detect impacts on a large stiffened composite structure. The inputs of the ANN were the measurements of 10 PZT sensors and the outputs were the impact location and the impact energy. However, the construction of the reference data set, consisting in applying multiple impacts on the structure, may not be affordable in some applications. Alternatively, Sharif-Khodaei et al. [10] generated numerical measurements with a finite element model of the structure to train the ANN. Yet, the discrepancies between the finite element model and the real structure may result in large localization errors. Eventually, it can be mentioned that triangulation techniques have been successfully validated on large aerospace structures [11, 12, 13]. Yet, the density

*Corresponding author
Email address: dimitri.goutaudier@gmail.com (Dimitri Goutaudier)

of the sensor network to achieve accurate impact localization may be prohibitive for an industrial application.

To overcome the difficulties of the wave-based techniques, a number of localization techniques based on the complete vibration response have been developed. Sweeping techniques consist in solving the inverse problem of force reconstruction through moving the estimated impact location [14, 15, 16]. The candidate that minimizes an error between model predictions and measurements is selected as the impact point. However, this approach is limited when the structure's dimensions are large as the number of potential impact locations significantly increases. Besides, the force reconstruction problem is ill-conditioned hence a regularization technique must be employed [17]. The selection of the regularization parameter is repetitive [18, 19] which can be too time consuming for a real-time impact identification. More advanced signal processing techniques based on the complete vibration response have also been employed to localize impact events on complex structures. Qiu et al. [20] used a time-reversal technique to estimate the impact locations on an aircraft wing box equipped with 24 PZT sensors. Kim et al. [21] used a normalized cross-correlation technique to localize impact events on a composite panel equipped with 4 FBG sensors.

The previous studies become limited with regard to the applicability for large and complex structures as the required number of sensors and the signal processing time significantly increase. In this paper, a long-range localization technique is proposed to achieve impact localization with a limited number of sensors. The applicability of the proposed technique does not depend on the structural geometry or the properties of the materials. Instead, the proposed technique relies on the knowledge of a few low frequency vibration modes of the structure that can be determined either experimentally or numerically [22]. The basic idea of the proposed approach is that the vibration modes are not excited in the same proportions depending on impact location. A few techniques are also based on this idea [23, 24] but experiments have only been conducted on beam-like structures. In addition, the choice of the vibration modes to be kept in the analysis is not addressed while it drives the accuracy of the impact localization. In this work, the authors describe a modal signature of the impact location. A criterion is presented to select appropriate vibration modes in the analysis. The proposed technique is validated on a commercial aircraft panel equipped with a sparse distribution of accelerometers. Experimental results show that the proposed technique achieves accurate impact localization even if the impact point is far from the nearest sensor of the network.

The paper is organized as follow. Section 2 describes the governing equation of the low frequency content of the impact response. Section 3 presents a modal signature of the impact location. Section 4 describes the proposed signal processing technique to achieve a long-range impact localization from a sparse distribution of sensors. Eventually, section 5 is dedicated to the experimental validation of the proposed impact identification methodology on a large composite aircraft panel.

2. Low frequency content of the impact response

Consider a plate-like structure, initially at rest, undergoing a transverse impact at time t_0. The impact energy is assumed high enough to produce global vibrations of the structure. Thereby, the transverse response $q(t)$, measured at any sensor location, is typically divided in three phases as follow. The impact first generates elastic waves travelling in the structure. These waves reach the sensor location at some time t_1 (TOA) and keep propagating in phase (II). After various reflections, these waves superimpose, from time t_2, into vibration modes in phase (III). The oscillatory response is ultimately damped due to different types of friction that dissipate the energy. These three phases are depicted in Figure 1.

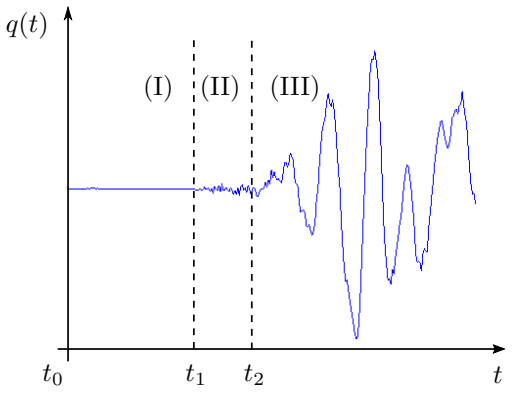

Figure 1: Illustration of the three phases in an impact response: (I) rest (II) wave passages (III) modal superposition.

The low frequency content of phase (III) can be described with a superposition of vibration modes as in [25]:

$$\tilde{q}(t) = \sum_{j=1}^{p} \phi_j(C)\phi_j(F)(f\psi * g_j)(t) \tag{1}$$

where C, F, f and $\psi(t)$ are respectively the sensor location, the impact point, the impact intensity and the unit load history. $\phi_j(M)$ denotes the mass-normalized mode shape of the j-th mode evaluated at some point M along the transverse direction. $(f\psi * g_j)(t)$ denotes the convolution product between the load history and the impulse response of the j-th modal coordinate. This latter is defined by:

$$g_j(t) = \frac{1}{\omega_j} e^{-\eta_j \omega_{0j} t} \sin(\omega_j t) \tag{2}$$

where $\omega_{0j} > 0$ and $\eta_j < 1$ are respectively the natural pulsation and the damping ratio of the j-th mode, and where $\omega_j = \omega_{0j}\sqrt{1-\eta_j^2}$.

There are mainly three advantages in using the low frequency content of the global vibrations. Firstly, it offers the possibility to achieve a long-range localization of the impact point as follow. The image of the impact location F in (1) is clearly a list of modal ponderations $\phi_j(F)$. These latter can be sensed far from the impact point, as long as the sensor is not located on a modal node ($\phi_j(C) \neq 0$). An inverse technique, described in section 4.3, is then employed to retrieve the impact location from specific modal ponderations. Secondly, the modal ponderations can be estimated with a robust procedure since they are in the vibration response for a long duration. On the opposite, triangulation techniques are based on the challenging identification of the instant t_1 [11]. Thirdly, sensors with a very high sampling frequency are expensive.

There is however an intrinsic difficulty in using the global vibrations for completly identifying an impact: the load history cannot be accurately reconstructed. This can be explained as follow. The impact response mainly consists in free vibrations of the structure since the impact duration T is usually very short. In fact, at an observation time $t \geq T$, relation (1) becomes:

$$\tilde{q}(t)_{t \geq T} = \sum_{j=1}^{p} f K_j \phi_j(C) \phi_j(F) g_j(t - \tau_j) \tag{3}$$

where the constants K_j and τ_j solely depend on the motion of the structure at the instant $t = T$. It becomes clear that the image of the load history in the free vibrations is a finite list of couples (K_j, τ_j). Consequently, the accurate variations of the load history cannot be captured in general. For this reason, we will focuss on capturing only a few important characteristics of the impact load, such as the impact time and the impact duration (see section 4.1).

3. Triangulation in the frequency domain: a modal signature of the impact location

Fundamentally, the localization of an impact applied on a plate-like structure consists in determining its two coordinates.

Triangulation techniques are usually developped in the time domain [6, 8, 15]. First, the TOAs of some elastic waves are captured at different sensor locations. Then, a wave velocity model is used to convert a TOA delay Δt into an iso-propagation line as described in [8]:

$$l_{j/i}(\Delta t) = \{M \mid t_1(C_j, M) - t_1(C_i, M) = \Delta t\} \tag{4}$$

where $t_1(C_i, M)$ represents the TOA at the sensor location C_i if the impact is applied at the point M. Each pair of TOA defines a specific delay Δt_{ji}. The iso-propagation lines are then derived to estimate the impact location:

$$\cap_{j \neq i} l_{j/i}(\Delta t_{ji}) = \{F\} \tag{5}$$

At least two iso-propagation lines are required to estimate the two coordinates of the impact point. Consequently, at least three sensors are required to compute at least two TOA delays.

In this study, a modal signature of the impact location is proposed instead of a time signature. The proposed approach can be seen as a triangulation technique in the frequency domain as follow. First, a model identification technique, described in section 4.1, is used to identify the modal ponderations through the following vector:

$$\mathbf{Z_F} = f.\left(\phi_1(F) \ ... \ \phi_p(F)\right)^T \tag{6}$$

Then, by analogy with triangulation techniques in the time domain, the idea with this formalism is to determine the set of the impact points that would excite two vibration modes in a given proportion λ. This leads to the concept of iso-proportion line defined by:

$$L_{j/i}(\lambda) = \{M \mid \phi_j(M) = \lambda \phi_i(M)\} \tag{7}$$

In particular, $L_{j/j}(0) = \{M \mid \phi_j(M) = 0\}$ is the nodal line of the j-th vibration mode, noted $L_j(0)$ in the following. Note that relation (7) does not depend on the sensor locations unlike relation (4). This is the key point of the long-range localization strategy presented in section 4.

It can be shown from relation (6) that the impact occurred at an intersection point of specific iso-proportion lines:

$$F \in I(F) \tag{8}$$

with:

$$I(F) = \begin{cases} \cap_{j=1}^{p} L_j(0) & \text{if } \phi_j(F) = 0 \text{ for any } j \in [\![1, p]\!] \\ \cap_{j=1, j \neq i}^{p} L_{j/i}(\lambda_{ji}) & \text{if } \phi_i(F) \neq 0 \text{ for some } i \in [\![1, p]\!] \end{cases} \tag{9}$$

where $\lambda_{ji} = \phi_j(F)/\phi_i(F)$ is the ratio between the j-th and i-th components of $\mathbf{Z_F}$.

In some cases, it exists a vibration modes family of the structure such that:

$$I(F) = \{F\} \tag{10}$$

This is notably the case for a simply supported isotropic plate as depicted in Figure 2.

In general, however, it is likely that the set of intersection points $I(F)$ is not solely reduced to the impact point F. For this reason, a tool is presented in section 4.2 to determine the areas of the structure that are covered by a given vibration modes family.

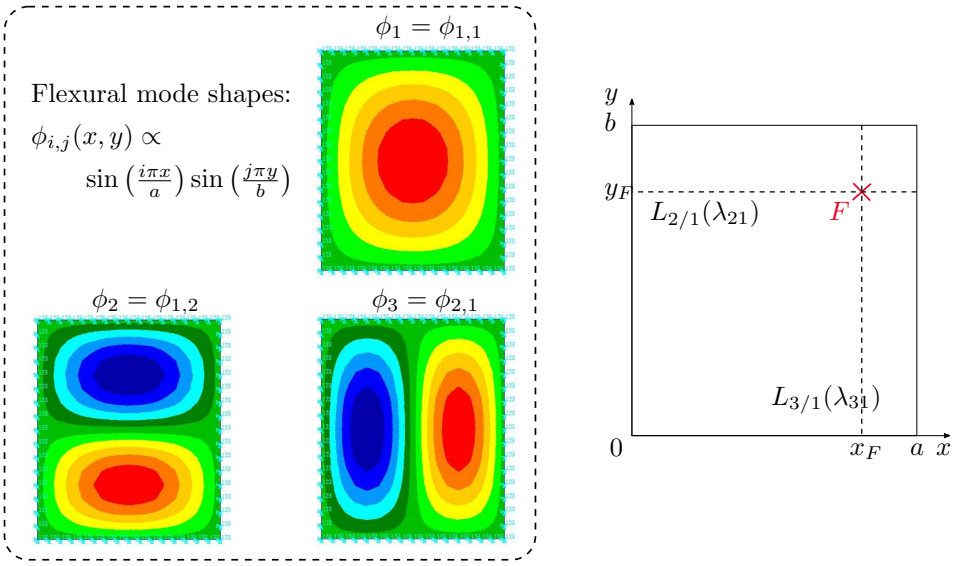

Figure 2: Iso-proportion lines of a simply supported isotropic plate intersecting at the impact location only.

4. Long-range impact identification strategy

The proposed impact identification strategy is divided in three steps:

Model identification: The unit load history and the modal ponderations are identified from the sensor measurements.

Reverse link: The impact location and its intensity are retrieved from the modal ponderations.

Data fusion: The individual localization results of each sensor of the network are combined.

4.1. Model identification

An acceleration response model $\tilde{a}(t)$ is used since accelerometers are generally smaller than displacement sensors and do not require a reference point. By separating the terms depending on (C, ψ) from the terms depending on (F, f), and by derivating twice with respect to time, equation (1) becomes:

$$\tilde{a}(t) = \ddot{\mathbf{L}}_\psi(t).\mathbf{Z_F} \tag{11}$$

where $\mathbf{Z_F}$ is defined by relation (6) and:

$$\ddot{\mathbf{L}}_\psi(t) = \left(\phi_1(C)\ddot{h}_1(t) \ ... \ \phi_p(C)\ddot{h}_p(t)\right) \tag{12}$$

with $h_j(t) = (\psi * g_j)(t)$. As mentioned in section 2, using the low frequency content of the vibration response results in the impossibility of accurately reconstructing the unit load history $\psi(t)$. Instead, we shall focuss on capturing the impact time t_0 and its duration T through fitting a parametric half-sine law as in [26]:

$$\psi(t_0, T, t) = \begin{cases} \sin\left(\pi\frac{t-t_0}{T}\right) & \text{if } t \in [t_0, t_0+T] \\ 0 & \text{elsewhere} \end{cases} \tag{13}$$

Alternatively, an impulse model can be used to quickly assess the impact time:

$$\psi(t_0, t) = \delta(t - t_0) \tag{14}$$

where $\delta(t)$ is a Dirac function centered in $t = 0$. Note that $h_j(t) = g_j(t - t_0)$ in this case.

The model identification is achieved through a minimization procedure where the design variables are t_0, T and $\mathbf{Z_F}$. The objective function is a quadratic distance between the measurements $a(t_i)$ and the predictions $\tilde{a}(t_i)$. After the resolution of the optimization problem, ψ is identified, but the impact location F and its intensity f are still to be determined from the vector $\mathbf{Z_F}$.

4.2. Coverage of a vibration modes family

In practice, the iso-proportion lines (7) cannot be derived since the mode shapes are usually not analytically known. As a result, the impact location cannot be estimated from $\mathbf{Z_F}$ by using the localization property (8). Instead, a $N \times p$ modal matrix $\mathbf{\Phi}$ is available. Its columns are the discretized mode shapes evaluated along N transverse DOFs of the structure. Let's note $\phi^*_\mathbf{i}$ the columns of $\mathbf{\Phi}^T$, called modal ponderation vectors in the following, so that:

$$\mathbf{\Phi}^T = [\phi^*_\mathbf{1}|...|\phi^*_\mathbf{N}] \tag{15}$$

Each DOF is mapped to a modal ponderation vector:

$$\text{DOF}_i \mapsto \phi^*_\mathbf{i} \tag{16}$$

Let's abusively note $F \in [\![1, N]\!]$ the index of the impacted DOF. Then, the vector $\mathbf{Z_F}$, called Amplified Modal Ponderation Vector (AMPV) in the following, is given by:

$$\mathbf{Z_F} = f.\phi^*_\mathbf{F} \tag{17}$$

A procedure is presented in section 4.3 to retrieve the impact location F and its intensity f from an estimation $\hat{\mathbf{Z}}_\mathbf{F}$ of the AMPV. More theory is however presented in the following to motivate this inverse procedure.

Without any loss of generality, assume that $p = 3$ vibration modes of the structure are selected in the analysis. The normalized columns of $\mathbf{\Phi}^T$ can be distributed within the half of a 3D unit sphere, even if that means turning upside down some of them, as depicted in Figure 3.

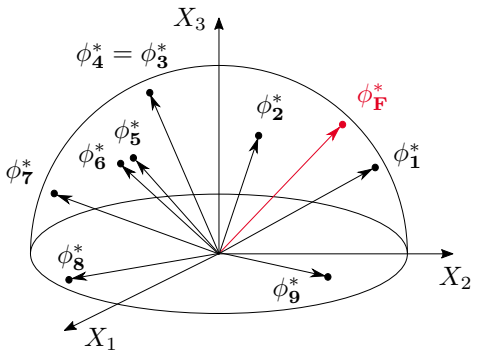

Figure 3: Geometrical representation of the modal ponderation vectors $\phi^*_\mathbf{i}$ in the case $p = 3$ and $N = 10$. Each DOF is mapped to a modal ponderation vector: $\text{DOF}_i \mapsto \phi^*_\mathbf{i}$.

In some areas of the sphere, some points might coincide, meaning that a same modal ponderation vector $\phi^*_\mathbf{i}$ is associated to two distinct DOFs of the structure. In other areas, however, all the points may be distinct, meaning that each DOF keeps its individuality in terms of modal ponderations:

$$\text{DOF}_i \leftrightarrow \phi^*_\mathbf{i} \tag{18}$$

Yet, even if all the points on the sphere are distinct, it is also likely that two close points are not associated to two close DOFs of the structure. A tool is therefore proposed in the following to anticipate these cases.

Let's note $\epsilon > 0$ a proximity tolerance. Each $\phi^*_\mathbf{i}$ has a specific deviation angle $\theta_i \in [0, \pi/2]$ with respect to the direction of $\phi^*_\mathbf{F}$. Let's define a collinearity tolerance $\theta(F)$ for the point F as follow: all the DOF_i satisfying $\theta_i \leq \theta(F)$ are associated to points of the structure that are ϵ-close to F. Now let's define the largest collinearity tolerance for the point F by $\theta_\epsilon(F) = \sup\, \theta(F)$. Therefore, the mapping

$$M \mapsto \theta_\epsilon(M) \tag{19}$$

indicates the areas that are best covered by the selected vibration modes family (higher values of θ_ϵ). An example of such a plot is presented in section 5.2.

4.3. Localization procedure

Assume that the selected vibration modes family covers the impacted area for a given proximity tolerance $\epsilon > 0$, meaning that $\theta_\epsilon(M)$ is not null for any point M in this area. The estimated AMPV $\hat{\mathbf{Z}}_\mathbf{F}$ may not be exactly collinear to $\phi^*_\mathbf{F}$ as in relation (17). Consequently, the reverse link (18) might not be applicable. The proposed localization procedure is as follow:

Inputs : $\mathbf{\Phi}$, $\hat{\mathbf{Z}}_\mathbf{F}$, $\gamma > 1$

Step 1: Compute the deviation angles $\hat{\theta}_i \in [0, \pi/2]$ between the vectors $\phi^*_\mathbf{i}$ and the direction of $\hat{\mathbf{Z}}_\mathbf{F}$.

Step 2: Compute $\hat{\theta}_m = \min_i \hat{\theta}_i$.

Step 3: Identify $I \subset [\![1, N]\!]$ such that $\hat{\theta}_i \leq \gamma \hat{\theta}_m$ for any $i \in I$.

Step 4: Associate a point F_i of the structure for each $i \in I$ (candidate impact points).

Step 5: Compute the collinearity factors for each $i \in I$ (candidate impact intensities):

$$f_i = \frac{(\phi^*_\mathbf{i})^T . \hat{\mathbf{Z}}_\mathbf{F}}{\|\phi^*_\mathbf{i}\|_2^2} \tag{20}$$

Outputs: Set of candidate parameters (F_i, f_i)

Step 3 selects the DOFs associated to the vectors $\phi^*_\mathbf{i}$ that are most collinear to $\hat{\mathbf{Z}}_\mathbf{F}$. Since $\theta_\epsilon(F)$ is not null, the proposed procedure can resist estimation errors on the modal ponderations for localizing the impact point.

4.4. Data fusion

Consider that the structure is equipped with a network of accelerometers located at some points C_j. The model identification step, described in section 4.1, can be performed with each accelerometer measurements $a(C_j, t)$. All the estimated AMPVs $\hat{\mathbf{Z}}^{(j)}_\mathbf{F}$ can then be used to improve the localization performances.

A generalized intersection technique is proposed as follow. First, define for each accelerometer an individual area of localization A_j:

$$a(C_j, t) \mapsto \hat{\mathbf{Z}}^{(j)}_\mathbf{F} \mapsto A_j \tag{21}$$

where A_j is the set of the mesh cells containing at least one DOF identified from $\hat{\mathbf{Z}}^{(j)}_\mathbf{F}$. Then, find the subset $\hat{A}$ of the cells that have been identified by the largest number of sensors. This technique discards the localization results that are too deviated from the majority.

In addition, the use of a sensor network allows to get a better first estimate of the impact time by determining the sensor responding first. Consequently, the estimation of the parameter t_0 in the model identification step is strongly eased.

5. Impact monitoring demonstration on a large aircraft composite panel

The main objective of this work is to develop an impact localization technique that is applicable to a large composite structure equipped with a sparse distribution of sensors. In this context, classical triangulation techniques become hardly applicable given that two sensors of the network are separated with a long distance. The propagation media between the impact point and the sensor locations is then likely to exhibit various obstacles to wave propagation (stringers, holes, assembly interfaces, etc.).

To overcome this difficulty, the proposed approach consists in extracting specific modal ponderations from the vibration measurements as a signature of the impact location (see section 3). The key point is to use the global vibration response of the structure that can be sensed at any location, provided that the impact energy is sufficient.

The purpose of this section is to demonstrate the applicability of the proposed approach on an industrial composite structure with complex features.

5.1. Specimen and set-up

The specimen was a 9.24m×2.40m stiffened composite panel manufactured by Airbus (typical of a production part). There were 13 stiffeners in x-direction and 7 in y-direction. The panel had also three holes surrounded by rectangular composite reinforcements (see Figure 4). The panel was simply supported on six wood blocks and its extremities were strapped to prevent eventual rebounds during the impact tests.

Eight accelerometers PCB-356B21 were glued to the external surface of the panel. The impacts were applied on mid bays only with a hand-held impact hammer PCB-086D05. The software LMS Test Lab 15A was used to record the impact load history and the acceleration signals with a sampling frequency of 5.12kHz and an acquisition time of 0.755s.

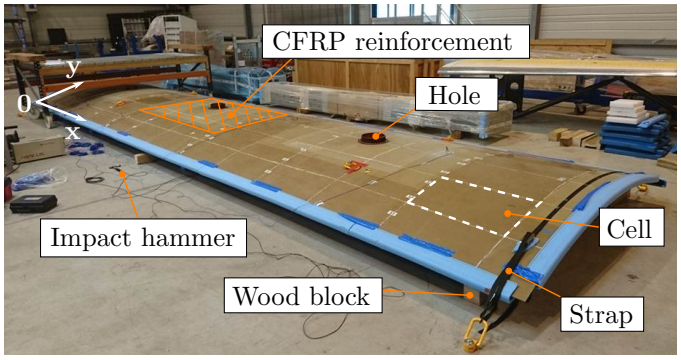

Figure 4: Description of the experimental set-up.

5.2. Modal analysis

An Experimental Modal Analysis (EMA) of the structure was performed prior to the impact tests with the software LMS Test Lab 15A [27]. A tap testing technique was used to identify 7 vibration modes within the frequency band 10-50Hz. The results of the EMA are summarized in Figure 5. In particular, mode shape #4 shows that the structure was not exactly symmetric. Figure 6 displays the accelerometer locations C_1 to C_8 and the main nodal lines of the identified vibration modes.

The mapping (19) with $\epsilon = 43$cm is displayed on Figure 7. The blue areas (low values of θ_ϵ) are sensitive to estimation errors on the modal ponderations. On the opposite, the red areas (high values of θ_ϵ) are robust to estimation errors. Therefore, it is expected to obtain lower localization performances for impacts applied in the blue areas of the panel.

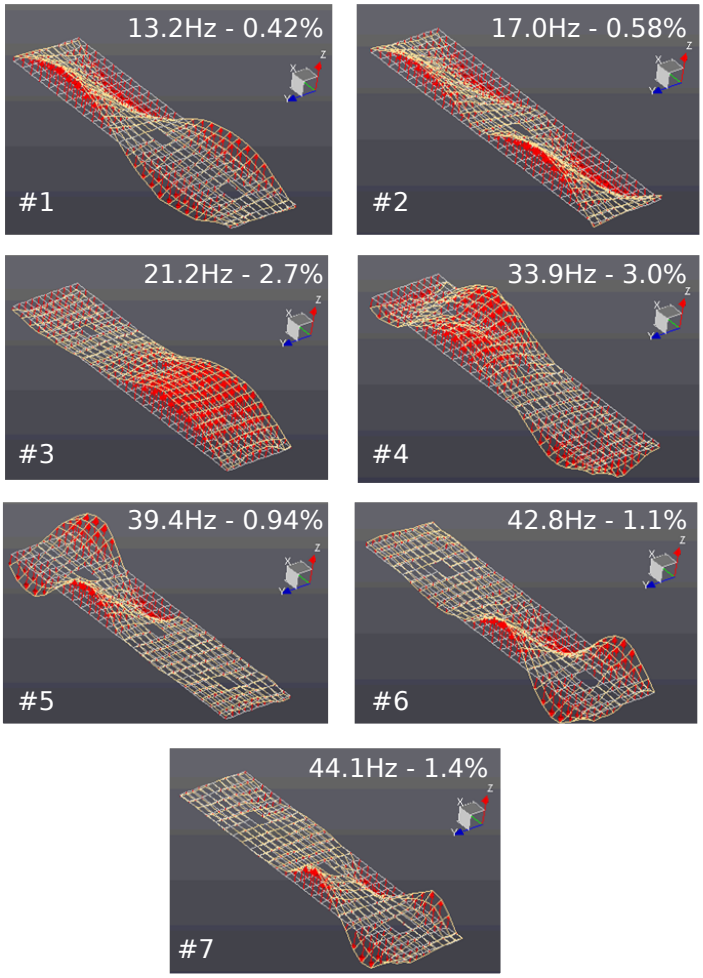

Figure 5: Modal properties of the structure within 10-50Hz (mode shape, natural frequency and damping ratio). Results of an Experimental Modal Analysis performed with a tap testing technique.

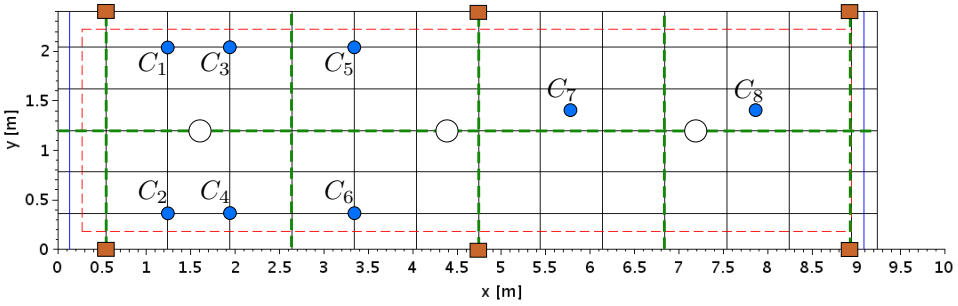

Figure 6: Locations of the accelerometers (brown rectangle: wood block, blue line: strap, red area: impacted zone, green line: nodal line).

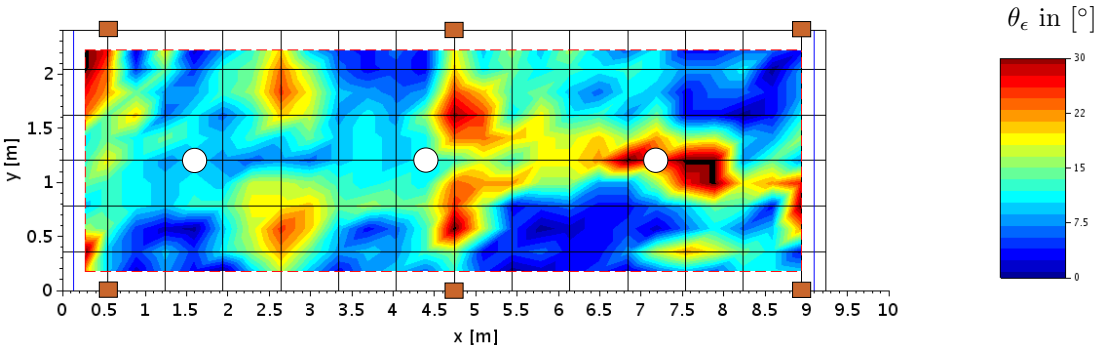

Figure 7: $M \mapsto \theta_\epsilon(M)$ with $\epsilon = 43$cm. Red zones are more robust to estimation errors on modal ponderations for localizing the impact point.

5.3. Implementation

The impact identification program was implemented with Scilab 5.5.2. The model identification step, presented in section 4.1, was performed as follow. The objective function to be minimized was:

$$J(\boldsymbol{\alpha}, \mathbf{Z_F}) = \sum_{i=1}^{n} (\tilde{a}(\boldsymbol{\alpha}, \mathbf{Z_F}, t_i) - a(t_i))^2 \tag{22}$$

were $\tilde{a}(t)$ is defined by relation (11) and $\boldsymbol{\alpha}$ is the list of parameters in the selected load model: (t_0, T) for the half-sine model (13) and t_0 only for the Dirac model (14).

First, the impact time t_0 was roughly estimated with the sensor responding first. A threshold technique based on the acceleration measurements was used (5% of the maximum amplitude). Let's note τ this first estimation. Then, pre-defined values of the parameters were tested with realistic values (see Table 1):

$$t_0^{(j)} = \tau + j\Delta t_0 \tag{23}$$

$$T^{(k)} = T_m + k\Delta T \tag{24}$$

Note that the minimization of (22) with a pre-defined value of $\boldsymbol{\alpha}$ is a well-known linear least-squares minimization problem. The couple $(\hat{\boldsymbol{\alpha}}, \hat{\mathbf{Z}}_\mathbf{F})$ minimizing the objective function was selected as the solution.

Eventually, the estimated AMPV $\hat{\mathbf{Z}}_\mathbf{F}$ was used to determine the candidate parameters (F_i, f_i) with the localization procedure described in section 4.3. To ease the visualization of the localization results on the planar representation of the panel (see Figure 6), a single estimate $(\hat{F}, \hat{f})$ was computed from the candidates (F_i, f_i) with a barycenter technique:

$$\begin{pmatrix} \hat{F} \\ \hat{f} \end{pmatrix} = \sum_{i=1}^{m} w_i \begin{pmatrix} F_i \\ f_i \end{pmatrix} \tag{25}$$

with $w_i = \cos(\hat{\theta}_i) / \sum_{k \in I} \cos(\hat{\theta}_k)$ to give more weight to candidates with small $\hat{\theta}_i$.

t_0		T		
τ	j	T_m	ΔT	k
Threshold	$-20 \to 10$	0.5ms	0.5ms	$1 \to 10$

Table 1: Load history model parameters

5.4. Localization results

It is a remarkable advantage of the proposed approach that the model identification step can be performed with the measurements of one sensor only. Recall that classical triangulation techniques require at least three sensors to determine the impact location on a plate-like structure. Both the single-sensor and the multi-sensors approaches were tested.

The impacts were applied at the center of the cells depicted in Figure 4 (mid bay). A localization was deemed successful if the localization error was lower than $\epsilon = 43$cm. The

Dirac model (14) was used to investigate the influence of the sensors selection on the localization performances.

Table 2 summarizes the results of the single-sensor approach. The opposite sensors (C_1, C_2) and (C_3, C_4) did not provide similar localization performances. This could be due to the assymmetry of the structure described in section 5.2. No clear explanation has been found to anticipate the localization performances depending on the accelerometer location. Yet, it is remarkable that the success rate of ϵ-localization reached 88% with the accelerometer located in C_2. In particular, the impact diametrically opposed to the sensor location (top/right corner of the panel) was successfully localized (see Figure 8). In addition, only three identifications failed (red crosses). Therefore, the proposed single-sensor approach is validated on this complex structure.

Sensor	C_1	C_2	C_3	C_4
Loc. (/48)	11	42	24	34
Success	23%	88%	50%	71%

Sensor	C_5	C_6	C_7	C_8
Loc. (/48)	17	17	23	2
Success	35%	35%	48%	4%

Table 2: Localization results with the single-sensor approach (number of successful ϵ-localizations/48 and success rate).

The single-sensor approach is however hardly applicable in operating conditions. If a sensor malfunctions, because of an improper calibration for instance, the localization results might be erroneous. To prevent this risk, a solution is to use at least 3 sensors. Table 3 summarizes the results obtained with different combinations of sensors. With this approach, the localization performances are not correlated with the number of sensors in the network (stabilization at 77% success). However, the number of failed identifications is strongly decreased, meaning that the multi-sensors approach is more reliable for identifying impact events. For instance, 100% of the applied impacts were identified with (C_2, C_3, C_4) (see Figure 9). Hence the strongly erroneous localization results of C_3 were successfully discarded by using the intersection technique described in section 4.4.

Combination	Loc. (/48)	Success
C_2, C_3, C_4	37	77%
C_2, C_3, C_4, C_7	36	75%
C_2, C_3, C_4, C_5, C_7	36	75%
$C_2, C_3, C_4, C_5, C_6, C_7$	37	77%
$C_1, C_2, C_3, C_4, C_5, C_6, C_7$	37	77%
$C_1, C_2, C_3, C_4, C_5, C_6, C_7, C_8$	37	77%

Table 3: Localization results with the multi-sensors approach (number of successful ϵ-localizations/48 and success rate).

Eventually, note that the lowest localization performances correspond to the impacts applied in the bottom/right quarter of the panel. This can be explained by the lowest values of θ_ϵ in this area (see the blue zone in Figure 7).

5.5. Reconstruction results

The half-sine model (13) was used to investigate the ability of the proposed approach to reconstruct the load history. The estimated impact amplitude, impact duration and impulse (integral over time) have been compared to the measured values. The results are summarized in Table 4. The impulse was less correctly estimated than expected (32.3% relative error). Indeed, the localization results with the impulse model supported that the impact durations were short enough to assume a Dirac-like impact (with respect to the dynamics of the selected vibration modes). However, the proposed approach is efficient for estimating the impact duration and the impact intensity, with respectively 19.0% and 29.2% of average relative error.

Load parameter	t_0	T	f	i
Av. error	1.34ms	19.0%	29.2%	32.3%

Table 4: Average errors of the estimated load parameters. i=impulse (integral over time). Results of the single-sensor approach with C_2.

For instance, Figure 10a shows the reconstruction of the force applied in (5.79m,1.83m) with the measurements of the accelerometer located in C_2. Figure 10b shows the frequency spectrum reconstruction of the associated acceleration signal. The frequency band 10-50Hz was not perfectly reconstructed (see the third modal ponderation). Yet, the proposed procedure is robust enough to identify the impact with estimation errors.

It should be mentioned that, in most cases, many shapes of the load model led to a similar frequency spectrum reconstruction. Figure 11 shows a family of load shapes leading to less than 2% more of the identified minimum of the objective function. This phenomenon can be explained as follow. Only low frequency vibration modes were selected in the analysis (<50Hz) while frequencies up to 250Hz were significantly excited. Hence most of the acceleration amplitude was due to higher order modes. As a result, the objective function was almost flat and various combinations of the load parameters could lead to a similar reconstruction of the acceleration data.

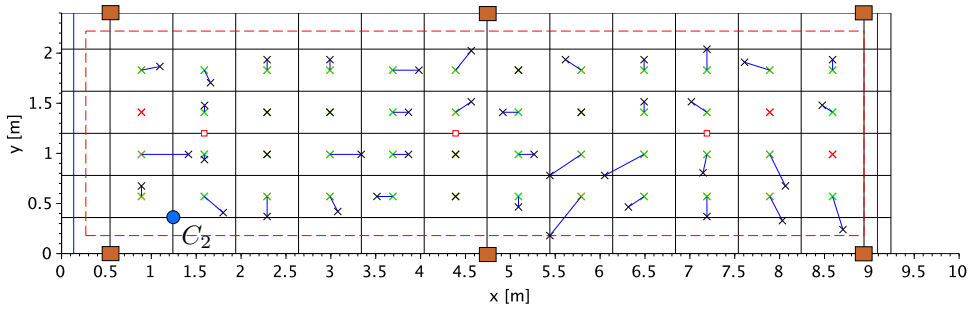

Figure 8: Localization map with C_2 only (green cross: impact location, black cross: estimate, red cross: failed identification).

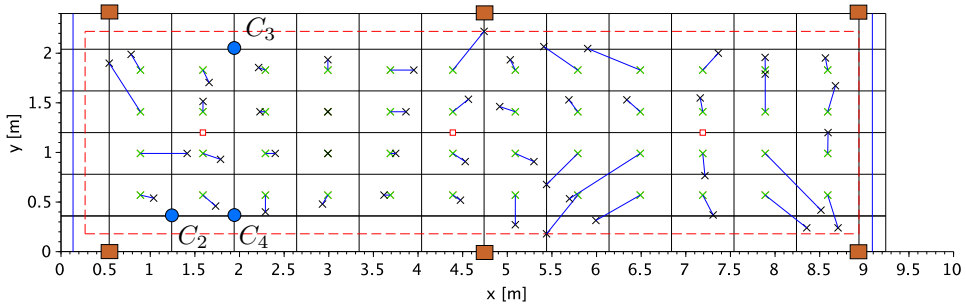

Figure 9: Localization map with (C_2, C_3, C_4). All the applied impacts are identified, even if the localization performances are globally lower than with the single-sensor approach.

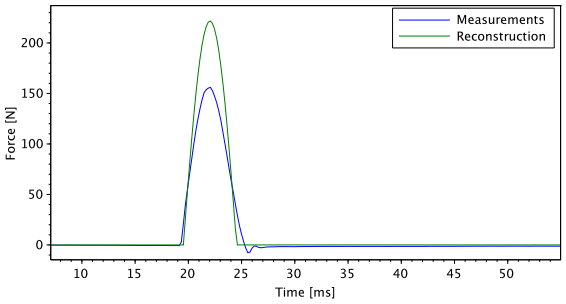

(a) Reconstruction of the load history with the half-sine model.

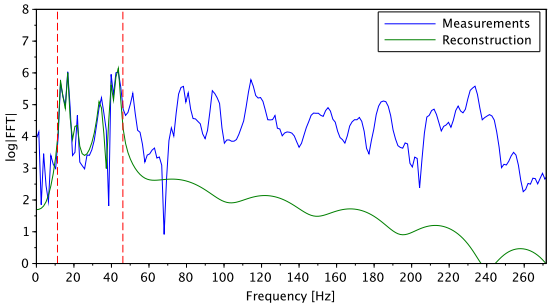

(b) Frequency spectrum reconstruction of the measured acceleration signal.

Figure 10: Identification of the impact applied in (5.79m,1.83m) with the measurements of the accelerometer located in C_2.

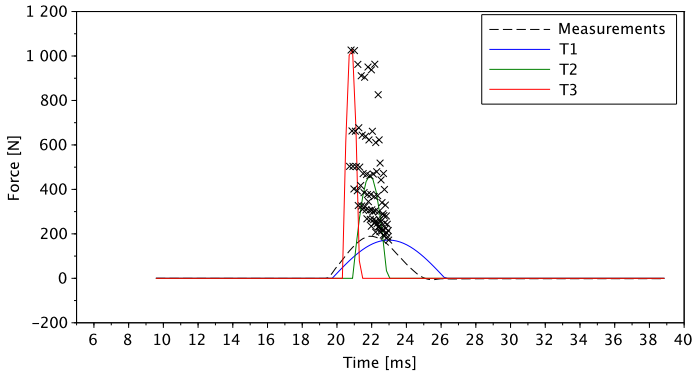

Figure 11: Family of load shapes reconstructing the measured data within 2% of the objective function minimum. Detailed plot of three candidate load shapes with $T_3 < T_2 < T_1$. The black crosses represent the peaks of the other candidate load histories.

6. Conclusion

A frequency domain triangulation technique was proposed to localize impact events on a composite structure with complex features. Instead of capturing the TOAs of some elastic waves, specific modal ponderations are estimated as a signature of the impact location. The structure's complexity is fully embedded in the low frequency vibration modes selected in the analysis, which can be determined either numerically of experimentally. In addition, compared with classical triangulation techniques, the proposed technique is consistent with a single-sensor approach. Consequently, a sensor far from the impact event can successfully localize the impact point. The proposed impact monitoring technique was successfully validated on a large aircraft composite panel equipped with a sparse distribution of accelerometers. The experimental results showed that a single accelerometer could efficiently localize impacts applied at any location on the panel.

References

[1] W. Cantwell, J. Morton, Comparison of the low and high velocity impact response of CFRP, Composites 20(6) (1989) 545:551.

[2] S. Abrate, Impact on laminated composite materials, Appl. Mech. Rev. 44(4) (1991) 155:190.

[3] P. Kumar, B. Rai, Delaminations of barely visible impact damage in CFRP laminates, Composite Structures 23(4) (1993) 313:318.

[4] A. Katunin, K. Dragan, M. Dziendzikowski, Damage identification in aircraft composite structures: A case studyusing various non-destructive testing techniques, Composite Structures 127 (2015) 1:9.

[5] J. Doyle, Wave propagation in structures, Springer, New York, 1989.

[6] G. Zhao, H. Hu, S. Li, L. Liu, K. Li, Localization of impact on composite plates based on integrated wavelet transform and hybrid minimization algorithm, Composite Structures 176 (2017) 234–243.

[7] J. Achenbach, Wave Propagation in Elastic Solids, North-Holland Publishing Company, Amsterdam, 1973.

[8] J. Frieden, J. Cugnoni, J. Botsis, T. Gmür, Low energy impact damage monitoring of composites using dynamic strain signals from fbg sensors – part i: Impact detection and localization, Composite Structures 94 (2012) 438–445.

[9] Y. Zhong, J. Xiang, H. Gao, Y. Zhou, Impact energy level assessment of composite structures using music-ann approach, Structural Control and Health Monitoring 23 (2016) 825–837.

[10] Z. Sharif-Khodaei, M. Ghajari, M. Aliabadi, Determination of impact location on composite stiffened panels, Smart Materials and Structures 21 (2012) 105026.

[11] J. Park, S. Ha, F.-K. Chang, Monitoring impact events using a system-identification method, AIAA Journal 47 (2009) 2011–2021.

[12] S. Yuan, Q. Bao, L. Qiu, Y. Zhong, A single frequency component-based re-estimated MUSIC algorithm for impact localization on complex composite structures, Smart Materials and Structures 24 (2015) 105021.

[13] M. Torres-Arredondo, C.-P. Fritzen, Impact monitoring in smart structures based on gaussian processes, 4th International Symposium on NDT in Aerospace (2012).

[14] L. Vladislav, R. Zemcik, T. Kroupa, J. Bartosek, Reconstruction of impact force on curved panel using piezoelectric sensors, Procedia Engineering 48 (2012) 367–374.

[15] S. Ahmari, M. Yang, Impact location and load identification through inverse analysis with bounded uncertain measurements, Smart Materials and Structures 22 (2013) 085024.

[16] Q. Li, Q. Lu, Impact localization and identification under a constrained optimization scheme, Journal of Sound and Vibration 366 (2016) 133–148.

[17] H. Inoue, J. Harrigan, S. Reid, Review of inverse analysis for indirect measurement of impact force, Applied Mechanics Reviews, American Society of Mechanical Engineers 54 (2001) 503–524.

[18] P. Hansen, Analysis of discrete ill-posed problems by means of the L-curve, Journal of the Society for Industrial and Applied Mathematics 34 (1992) 561–580.

[19] H. Choi, A. Thite, D. Thompson, Comparison of methods for parameter selection in tikhonov regularization with application to inverse force determination, Journal of Sound and Vibration 304 (2007) 894–917.

[20] L. Qiu, S. Yuan, X. Zhang, Y. Wang, A time reversal focusing based impact imaging method and its evaluation on complex composite structures, Smart Materials and Structures 20 (2011) 105014.

[21] J.-H. Kim, Y.-Y. Kim, Y. Park, C.-G. Kim, Low-velocity impact localization in a stiffened composite panel using a normalized cross-correlation method, Smart Materials and Structures 24 (2015) 045036.

[22] Z.-F. Fu, J. He, Modal analysis, Butterworth-Heinemann, 2001.

[23] J. Briggs, M.-K. Tse, Impact force identification using extracted modal parameters and pattern matching, International Journal of Impact Engineering 12 (1991) 361–372.

[24] B.-T. Wang, C.-H. Chiu, Determination of unknown impact force acting on a simply supported beam, Mechanical Systems and Signal Processing 17 (2003) 683–704.

[25] M. Géradin, D. J. Rixen, Mechanical Vibrations - Theory and Application to Structural Dynamics, Third Edition, Wiley, 2015.

[26] G. Yan, L. Zhou, Impact load identification of composite structure using genetic algorithms, Journal of sound and vibration 319(3-5) (2009) 869–884.

[27] LMS International, The LMS Test.Lab Modal Analysis manual - Rev 12A, 2012.